The Effect of Quench Rate on the Microstructure, Mechanical Properties, and Corrosion Behavior of U-6 Wt Pct Nb

K. H. ECKELMEYER, A. D. ROMIG, Jr., and L. J. WEIRICK

The effect of cooling rate on the microstructure, mechanical behavior, corrosion resistance, and subsequent age hardenability of U-6 wt pct Nb is described and discussed. Cooling rates in excess of 20 Ks^{-1} cause the parent γ-phase to transform martensitically to a niobium supersaturated variant of the α-phase. This martensitic phase exhibits low hardness and strength, high ductility, good corrosion resistance, and substantial age hardenability. As cooling rate decreases from 10 Ks^{-1} to 0.2 Ks^{-1}, fine scale microstructural changes (consistent with spinodal decomposition) occur to an increasing extent. These changes produce large increases in hardness and strength and large decreases in ductility, slight decreases in corrosion resistance, and slight changes in age hardenability. At cooling rates less than 0.2 Ks^{-1} the parent phase undergoes cellular decomposition to a coarse two-phase lamellar microstructure. This lamellar microstructure exhibits intermediate strength and ductility, substantially reduced corrosion resistance, and no age hardenability. An analysis of the cooling rates at the centers of water quenched plates indicates that fully martensitic microstructures can be obtained in plates as thick as 50 mm.

I. INTRODUCTION

URANIUM is used in a variety of applications because of its high density (19.1×10^3 kg/m^3) and its unique nuclear properties. Poor corrosion resistance and unfavorable combinations of strength and ductility, however, are difficulties which must be overcome in order to exploit this material in engineering applications. It is known that solid solution additions of elements such as niobium, titanium, and zirconium markedly improve uranium's resistance to corrosion and substantially alter its mechanical properties.[1-5] Unfortunately, these elements are extensively soluble only in the high temperature cubic γ-phase and almost completely insoluble in the low temperature orthorhombic α-phase. This difficulty can be avoided by heat treating uranium alloys in the γ-phase field (to form uranium alloy solid solutions) followed by rapid quenching to room temperature. The high cooling rate forces the γ-phase solid solution to transform martensitically to variants of the low temperature α-phase in which the alloying elements are retained in supersaturated solid solution. These metastable α-phase solid solutions exhibit far better corrosion resistance than unalloyed uranium. These solid solutions are highly supersaturated and are amenable to subsequent age hardening, permitting a wide range of mechanical properties through the selection of aging temperature and time. Application of these principles to the U-6 pct Nb alloy* can result in corrosion rates which are orders of magnitude lower than that of unalloyed uranium,[6] combined either with yield strengths as high as 1300 MPa[7] (six times that of unalloyed uranium), or with tensile elongations as high as 30 pct[7] (equivalent to that of high quality fine grained wrought unalloyed uranium).

*All compositions are given as weight percentages.

K. H. ECKELMEYER, Supervisor, Electron Optics and X-Ray Analysis Division 1822; A. D. ROMIG, Jr., Member of Technical Staff, Physical Metallurgy Division 1832; and L. J. WEIRICK, Member of Technical Staff, Corrosion Division 1841, are all with Sandia National Laboratories, P.O. Box 5800, Albuquerque, NM 87185.

Manuscript submitted April 15, 1983.

The equilibrium microstructure of U-6 pct Nb and the properties associated with material in this condition can be understood by referring to the uranium-niobium phase diagram shown in Figure 1.[8] At the solution treatment temperature of 1073 K all of the niobium is dissolved in the γ_1-phase. When cooled very slowly such that an approach to equilibrium is maintained, the γ_1-phase undergoes diffusional decomposition at 920 K to a two-phase structure consisting of essentially unalloyed α-uranium and niobium rich γ-phase. Material in this condition does not have good corrosion resistance[7] because the α-phase contains virtually no niobium in solid solution and because the two-phase structure gives rise to microscopic anodic and cathodic regions. Second-phase strengthening results in yield strengths of approximately 900 MPa, but tensile elongation is only about 12 pct.[9]

The microstructure and properties associated with quenched U-6 pct Nb are markedly different and far more

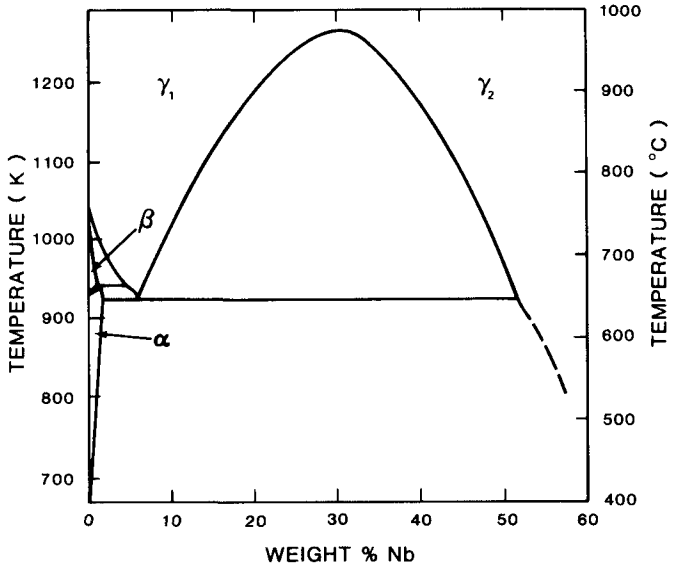

Fig. 1—The U-Nb equilibrium phase diagram.

desirable than the slow cooled U-6 pct Nb. Rapid cooling from the 1073 K solution treatment temperature suppresses diffusional decomposition and causes the γ_1-phase to transform martensitically to a supersaturated variant of the α-phase termed α''.[10,11] This α'' structure has excellent corrosion resistance because the niobium is uniformly distributed in solid solution. The extensively twinned thermoelastic martensitic microstructure of the α'' results in very low yield strength (approximately 200 MPa) and high tensile elongation (approximately 30 pct).[7] The fact that the α'' structure is supersaturated with niobium also enables it to be age hardened by heating it to temperatures where limited amounts of solid state diffusion can occur. Aging in the 423 K to 673 K range results in increases in yield strength to as high as 1300 MPa[7] due to very fine scale microstructural changes which have not yet been fully characterized. Overaging occurs at temperatures in excess of approximately 673 K[7] due to cellular decomposition to relatively coarse two-phase structures.

The U-6 pct Nb α'' martensite provides the best corrosion resistance and mechanical properties. The U-6 pct Nb alloy must be solution heat treated and quenched to obtain α'' martensite. The cooling rate must be sufficiently high to suppress completely diffusional decomposition of the γ_1-phase. Jackson has studied isothermal transformation in this alloy and has shown that the kinetics of γ_1-phase decomposition can be characterized by two C-curves.[12] The upper C-curve corresponds to monotectoid decomposition to a lamellar structure of an α-phase and a niobium enriched γ-phase. The nose of this curve is at approximately 803 K and 50 seconds. The lower C-curve corresponds to much finer scale microstructural changes which have not been extensively characterized, but which are described by Jackson to be highly localized microsegregation of niobium. The nose of this curve is at approximately 673 K and 100 seconds. If these diffusional decomposition modes are suppressed, athermal martensitic transformation to α'' begins at approximately 363 K and is complete at approximately 333 K.[12]

While this characterization of the kinetics of isothermal decomposition of the γ_1-phase was done some time ago, the logical next step of determining the effects of continuous cooling rate on microstructure and properties has not been carried out. Due to the absence of continuous cooling information U-6 pct Nb parts are traditionally water quenched from 1073 K as a convenient method by which 100 pct martensitic microstructures and the associated desirable properties can be obtained with confidence. The fact that the noses of the C-curves are at fairly long times, however, suggests that substantially less severe quenches would probably be equally effective. Less drastic quenches would be advantageous in that they would produce lower quench induced residual stresses and result in less distortion during subsequent machining. The object of the present study, then, is to characterize quantitatively the effects of cooling rate on the mechanical properties, corrosion behavior, and aging response of U-6 pct Nb and to interpret these effects in terms of microstructure.

II. EXPERIMENTAL

Material for this investigation was made at the Union Carbide Corporation Y-12 Plant. A 200 mm diameter ingot was produced by skull melting and vacuum arc remelting of high purity uranium and niobium starting materials. The ingot was sectioned into 114 mm and 178 mm high billets. These billets were vacuum homogenized at 1273 K for four hours and formed into 14 mm and 25 mm thick circular plates by a combination of upset forging and cross rolling in the γ_1-phase field. The chemical composition of this material is shown in Table I.

The effects of cooling rate on microstructure and properties were determined as follows. Heat treating blanks 14 mm × 14 mm × 114 mm and 2.5 mm × 25 mm × 114 mm were sawed from the plates. These blanks were solution treated at 1073 K and cooled to room temperature in various media (water, oil, forced air, still air, ash) to obtain a broad spectrum of cooling rates. The combinations of blank sizes and quench media used are shown in Table II. Holes were drilled to the centers of several heat treating blanks and Pt/Pt-10 pct Rh thermocouples were inserted and welded in place to enable measurement of center-line cooling rates during quenching. Tensile specimens with 6.35 mm diameter × 25.4 mm long gage sections were machined from the centers of identically heat treated blanks.* The tensile specimens were tested in dry air at a strain rate of 10^{-1} s^{-1}. All tensile results reported are the averages of two specimens. Additional blanks were identically heat treated and sectioned into samples for hardness, corrosion, X-ray diffraction, metallographic, and age hardening studies. Hardness tests were made using the Rockwell A scale so that a wide range of hardnesses could

*All blanks from which tensile specimens were machined were solution heat treated at 1073 K for three hours in vacuum in order to remove residual hydrogen and avoid possible hydrogen embrittlement effects. The time-temperature parameters were insufficient for significant grain growth.

Table I. Chemical Analysis of Experimental Material*

Niobium	5.9 pct
Hydrogen (bulk)	0.94 ppm
Oxygen	21 ppm
Nitrogen	38 ppm
Carbon	73 ppm
Aluminum	10 ppm
Copper	3 ppm
Iron	20 ppm
Silicon	35 ppm

*by weight

Table II. Experimental Quenching Conditions

Average Centerline Cooling Rate (Ks^{-1}, 973 to 873 K)	Section Size (mm)	Quench Medium
250	14 × 14	still water
105	25 × 25	still water
62	25 × 25	still oil
21	14 × 14	fine water spray
10	14 × 14	forced air
3.5	14 × 14	still air
2.2	25 × 25	still air
0.83	14 × 14	wood ash
0.18	25 × 25	wood ash
0.040	14 × 14	furnace cooled

be compared on a single plot. All hardness results represent the average of ten measurements made along the sample centerline. Three sets of corrosion samples were prepared. The first set was used in electrochemical tests, the second and third sets for corrosion response tests in moist air and moist nitrogen, respectively. The electrochemical test consisted of a rest potential measurement of a coupon submerged in an electrolyte of 10^{-3} M KCl and utilizing a standard calomel electrode (SCE). The second and third sets of coupons were exposed to moisture at a relative humidity of 95 pct at a temperature of 348 K in flowing air or nitrogen, respectively. The coupons were removed periodically and weight measurements taken.

Specimens for X-ray diffraction were polished through 1 μm diamond paste and examined with a diffractometer with CuKα monochromatic radiation. The sample centers were the areas examined. Metallographic specimens were mechanically polished through 0.3 μm Al_2O_3. Samples for bright-field illumination and scanning electron microscopy were electropolished and electroetched in 1:1 orthophosphoric acid: water at three volts. This etch also removed the effects of the mechanical polish. Samples for polarized light examination were anodized in 1:30 NH_4OH: ethylene glycol at 70 volts. Transmission electron microscopy/scanning transmission electron microscopy (TEM/STEM) samples were cut and ground to a thickness of <250 μm.

Self-supporting discs 3 mm in diameter were mechanically punched from the 250 μm wafers. The discs were further ground to a thickness of 25 to 50 μm. The edges of the discs were coated with etch stop and immersed in a solution consisting of 150 ml of methanol, 50 ml of butyl cellusolve, and 4 ml of perchloric acid employing a stainless steel cathode. Thinning was accomplished with the solution cooled to 258 K to 263 K at a potential of 20 V. The foils were analyzed with a JEM 100C TEM/STEM and a JEM 200CX TEM.

Samples for determination of age hardening response were vacuum aged at temperatures from 453 K to 873 K for six hours. After aging, these samples were subjected to hardness tests, optical metallography, and X-ray diffraction studies.

III. RESULTS

A. *Cooling Rates Obtained by Quenching*

The cooling rates obtained under the various quenching conditions are shown in Table II. These are reported as the average cooling rates between 973 K and 873 K in order to be consistent with the data previously reported for U-0.75 pct Ti.[13] Obviously, however, the instantaneous cooling rate for each quenching condition decreases with decreasing temperature.

B. *Effects of Cooling Rate on Mechanical Behavior*

The mechanical behavior results clearly indicate the existence of three regimes of quench rate dependence. The effect of cooling rate on hardness is shown in Figure 2. Very rapid cooling (250 Ks^{-1}) results in low hardness as would be expected of α'' martensite. No change in hardness occurs as cooling rate decreases from 250 Ks^{-1} to 20 Ks^{-1}. A substantial increase in hardness occurs with further reductions in cooling rate from 10 Ks^{-1} to 0.2 Ks^{-1}. Hardness then plateaus as cooling rate decreases below 0.2 Ks^{-1}. Throughout the remainder of this paper, then, the terms high cooling rate, intermediate cooling rate, and low cooling rate will frequently be used to refer to rates greater than 20 Ks^{-1}, between 20 Ks^{-1} and 0.2 Ks^{-1}, and less than 0.2 Ks^{-1}, respectively.

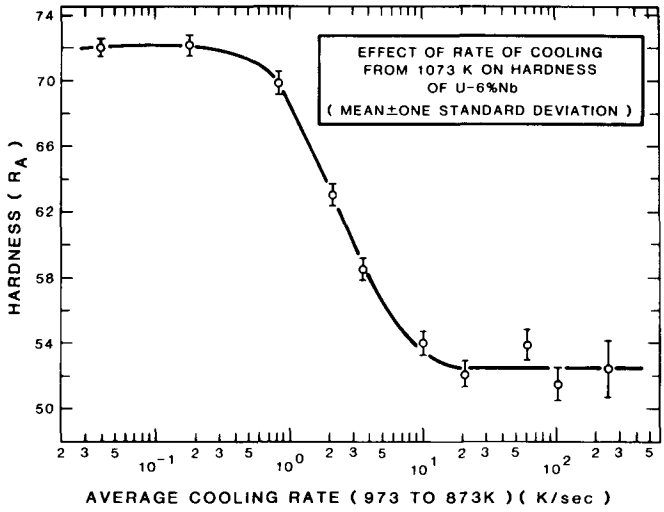

Fig. 2—The effect of cooling rate on hardness.

The effect of cooling rate on tensile properties is shown in Figure 3. The tensile results are quite consistent with the hardness trends. High cooling rates result in very low yield strength and extensive ductility. To a first approximation, tensile properties are independent of cooling rate in this regime. As cooling rate decreases from 10 Ks^{-1} to approximately 0.2 Ks^{-1}, the yield and ultimate strengths increase

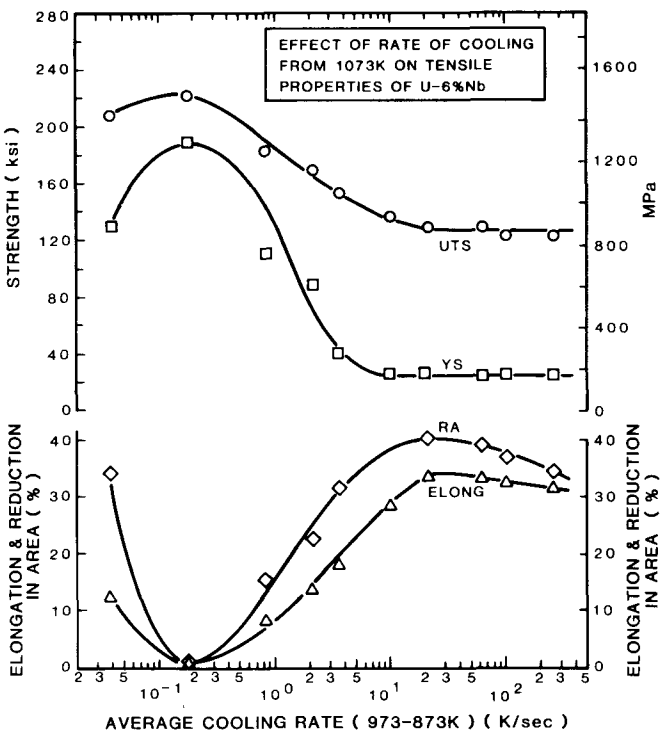

Fig. 3—The effects of cooling rate on tensile properties.

dramatically and ductility decreases to near zero. Further decreases in cooling rate below 0.2 Ks^{-1} result in substantial decreases in yield strength, slight decreases in ultimate strength, and substantial increases in ductility. It should be noted, however, that in material cooled at the lowest rate, the high ratio of reduction-in-area to elongation and examination of the tensile samples show that a substantial amount of the total elongation occurs in the localized area of necking and that uniform elongation is quite low.

Substantial changes in fracture surface appearance accompany these changes in tensile properties. Samples cooled at high rates fail entirely in shear, and the fracture surfaces consist of small numbers of large facets inclined at 45 deg to the tensile axes. Scanning electron microscope examination reveals these facets to be entirely covered with large but shallow dimples, as shown in Figure 4(a). This indicates that failure occurs by the nucleation, growth, and coalescence of microvoids. At intermediate cooling rates, failure continues to occur in a shear mode, but the fracture surfaces consist of a larger number of smaller facets. The dimple size also decreases with decreasing cooling rate and increasing ductility as shown in Figure 4(b). The same basic fracture mechanism is operating, but that increasing numbers of fracture nucleation sites are becoming active with increasing strength (a common phenomenon in many materials).[14] An abrupt change in fracture mode occurs at a cooling rate of 0.2 Ks^{-1} as shown in Figure 4(c). Fracture now occurs primarily in a tensile mode (perpendicular to the tensile axis), with small 45 deg shear lips being confined to the perimeter of the fracture surface. Most of the fracture surface is covered with dimples, as shown in Figure 4(c), but these are much smaller than in any of the previous samples. At the lowest cooling rate of 0.04 Ks^{-1}, fracture surface examination indicates primarily a quasicleavage mode of failure, as shown in Figure 4(d).

C. *Effects of Cooling Rate on Corrosion Behavior*

The effect of cooling rate on rest potential is shown in Figure 5. This behavior follows the mechanical property trends quite closely. Very rapid cooling results in a low rest potential as would be expected for a corrosion resistant

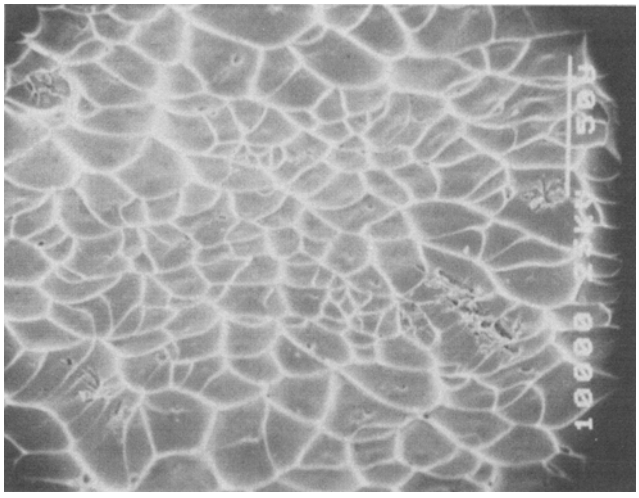

(*a*)

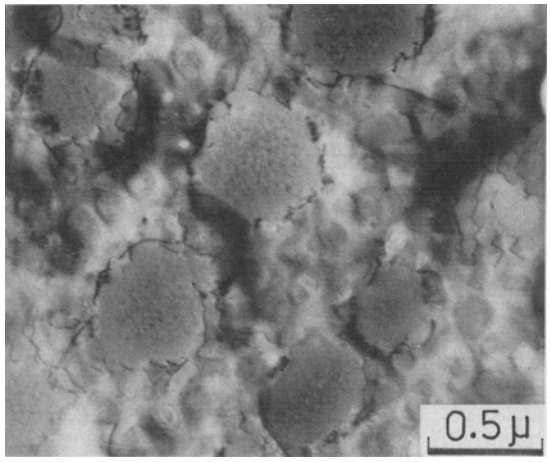

(*b*)

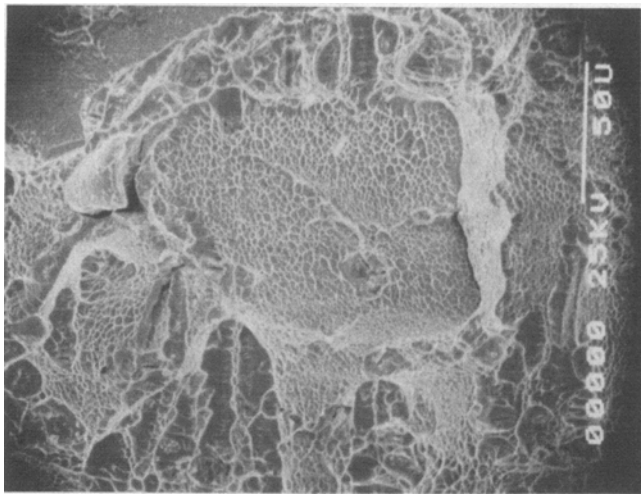

(*c*)

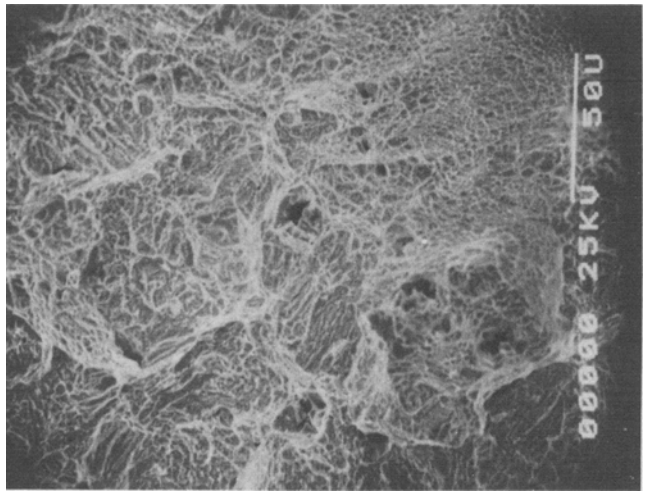

(*d*)

Fig. 4—Scanning electron micrographs of tensile fracture surfaces. (*a*) Cooling rate = 250 Ks^{-1}, (*b*) cooling rate = 0.83 Ks^{-1}, (*c*) cooling rate = 0.18 Ks^{-1}, and (*d*) cooling rate = 0.04 Ks^{-1}. Original magnification and μm scale bars are given on the photomicrographs.

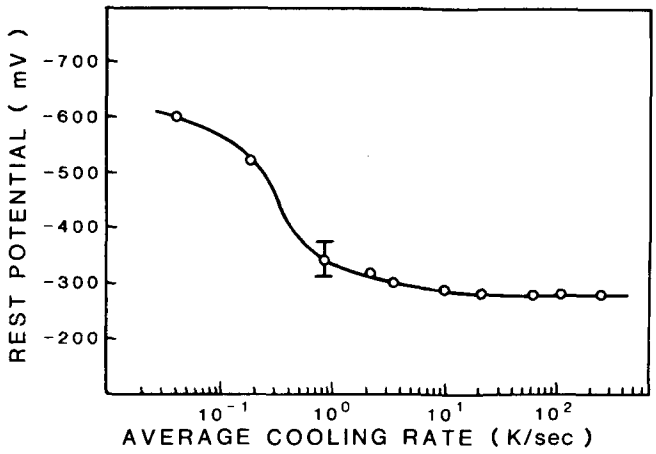

Fig. 5—The effects of cooling rate on rest potential in 10^{-3} M KCl. The error bar indicates the uncertainty in the potential measurement.

material. Rest potential is constant in the high cooling rate regime, and increases gradually with decreasing cooling rate in the 10 Ks^{-1} to 0.8 Ks^{-1} range. At low cooling rates the rest potential is substantially higher than that for any of the intermediate or high cooling rates. These results indicate that corrosion resistance is independent of cooling rate at cooling rates in excess of 20 Ks^{-1}, that a slight degradation of corrosion resistance occurs at cooling rates between 10 and 0.8 Ks^{-1}, and that a substantial decrease in corrosion resistance occurs at cooling rates below 0.8 Ks^{-1}.

Corrosion tests at 348 K in 95 pct relative humidity air and 95 pct relative humidity nitrogen confirm the inferences drawn from the rest potential results. No samples cooled at intermediate or high rates exhibited any surface tarnishing or measurable weight gain in up to 30 days. Samples cooled at low rates, however, formed a black surface coating during identical tests and exhibited an average weight gain of 0.010 mg/cm^2/day (~17 μm/y penetration for UO_2) (approximately 10 times the detection limit).

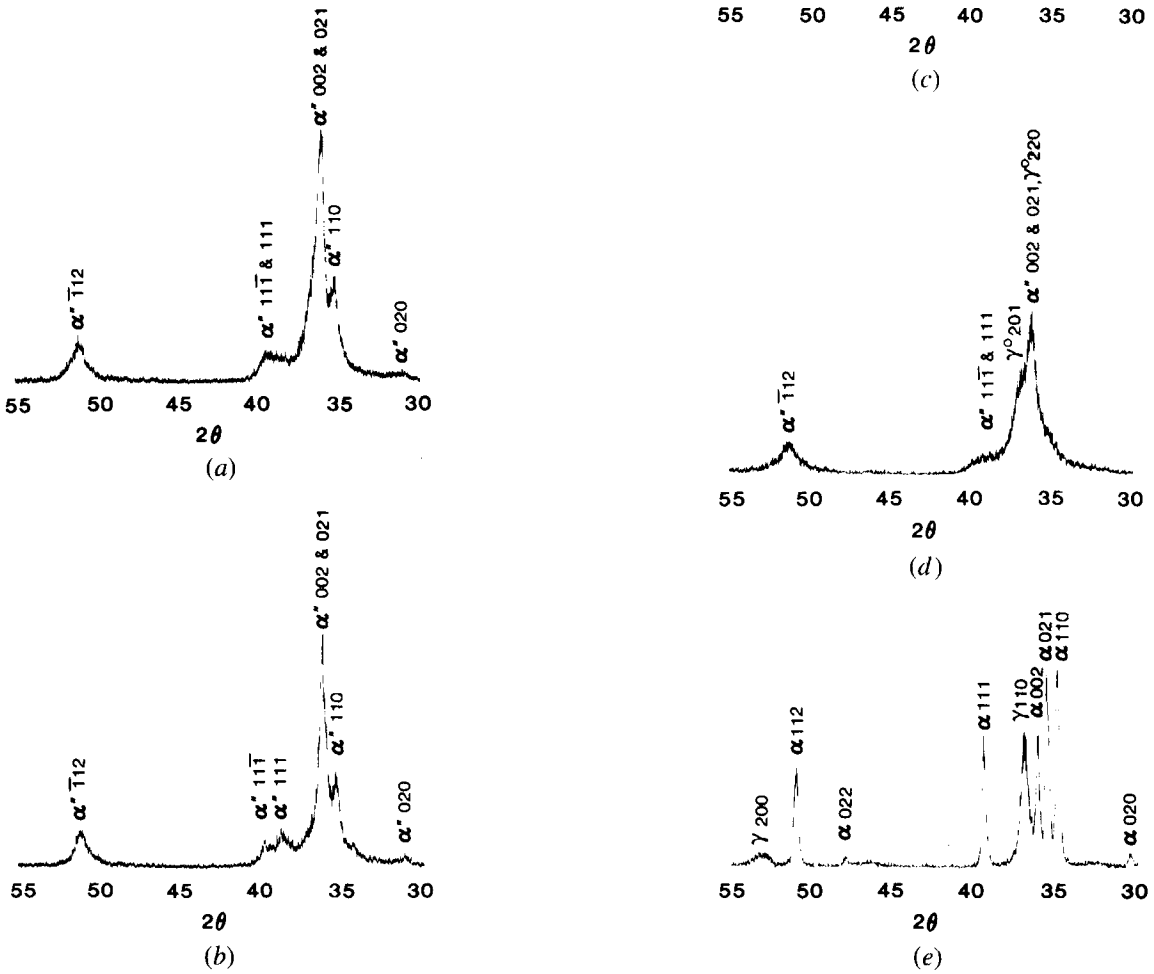

Fig. 6—The effect of cooling rate on X-ray diffraction patterns. (*a*) Cooling rate = 250 Ks^{-1}, (*b*) cooling rate = 10 Ks^{-1}, (*c*) cooling rate = 2.2 Ks^{-1}, (*d*) cooling rate = 0.83 Ks^{-1}, and (*e*) cooling rate = 0.04 Ks^{-1}.

D. *Effects of Cooling Rate on Microstructure*

X-ray diffraction was used to identify the phases produced by different cooling rates. The $30° < 2\theta < 55°$ regions of typical patterns are shown in Figure 6. All patterns obtained from samples cooled at 2 Ks^{-1} or greater can be clearly indexed as α''. The most rapidly cooled samples exhibit somewhat broadened diffraction peaks as can be seen in Figure 6(a). This broadening is believed to be due to strains produced by severe thermal gradients during the quench. As cooling rate decreases from 250 Ks^{-1} to 10 Ks^{-1}, the diffraction peaks sharpen as can be seen by comparing Figures 6(a) and 6(b). This is consistent with the expectation that decreasing quench severity should decrease the magnitude of quench induced strain because of lower thermal gradients and increased time for autorecovery. As cooling rate decreases below 10 Ks^{-1}, the diffraction peaks again broaden as can be seen by comparing Figures 6(b), 6(c), and 6(d). This is indicative of variations in interplanar spacings as could be caused either by the formation of coherent precipitates or the formation of spinodal compositional modulations. At a cooling rate of 0.8 Ks^{-1}, the diffraction pattern changes substantially as is shown in Figure 6(d). This pattern exhibits most of the primary features of α'', but the peaks are quite broad and the α'' (110) peak is prominent at $2\theta = 35.3°$, and does not appear above the shoulder of the broadened α'' (002) and (021) peak. In addition, a substantial peak appears on the shoulder of the α'' (002) and (021) peak at $2\theta = 36.9°$. This pattern is consistent with a structure consisting of α'' containing extensive coherent precipitation or compositional modulations, plus some $\gamma°$, a tetragonal variant of γ-phase.

At cooling rates of 0.2 Ks^{-1} and lower, the diffraction patterns reveal a mixture of $\alpha + \gamma$ phases as shown in Figure 6(e). The lattice parameters of the α phase are not perceptibly different from those of unalloyed α uranium, suggesting that very little niobium is in solid solution. The lattice parameter of the cubic γ phase is 3.442 ± 0.0075 Å based on the average of six measurements. According to Jackson's[15] equation, at. pct Nb = (3.475-a)/0.00175, indicating a niobium content of 9.5 ± 2.4 wt pct in the γ phase, much less than the ~54 pct that would be expected from the equilibrium phase diagram. This is consistent, however, with previous results indicating that a gamma phase of intermediate niobium content, termed γ_{1-2}, forms as a precursor to the equilibrium γ_2-phase which contains approximately 54 wt pct niobium.[16] If held for long times at elevated temperature, the γ_{1-2}-phase decomposes to equilibrium γ_2-phase plus additional α phase.[16] This effect has also been observed in work done at this laboratory.

The microstructure of the most rapidly cooled material is shown in Figure 7. Bright-field illumination reveals primarily the prior γ grain boundaries and a small amount of substructure (Figure 7(a)). The banded α'' martensitic structure can be seen within the prior γ grains under polarized light illumination (Figure 7(b)). Transmission electron microscopy reveals the extensive internal twinning that is common to this type of martensite (Figure 7(c)). As cooling rate decreases from 250 Ks^{-1} to 20 Ks^{-1}, the only microstructural change which occurs is a gradual increase in the amount of substructure within the prior γ grains. By 20 Ks^{-1} there is a well-defined subgrain network present as

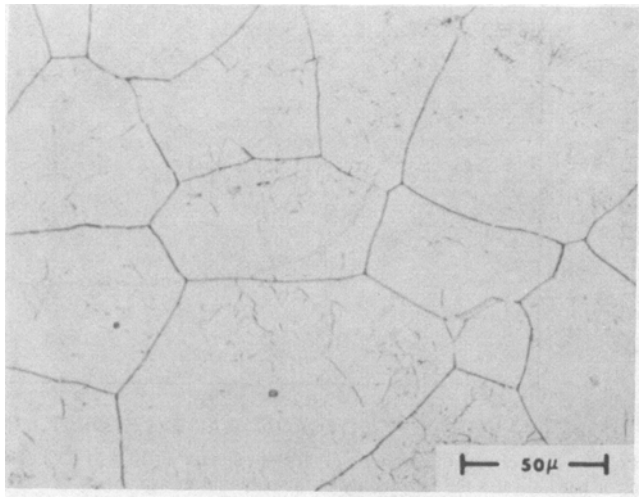

(*a*)

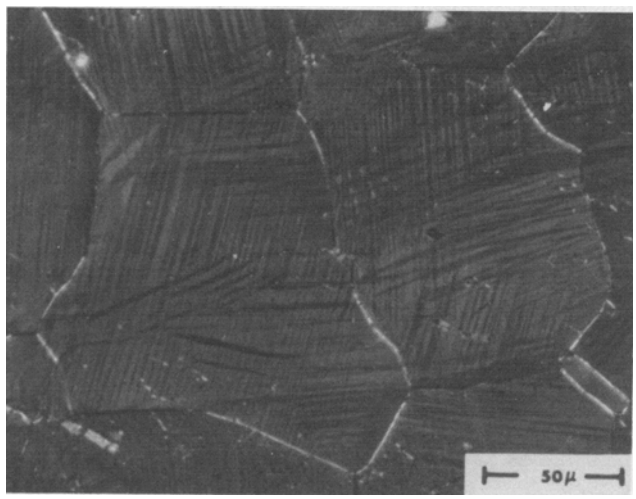

(*b*)

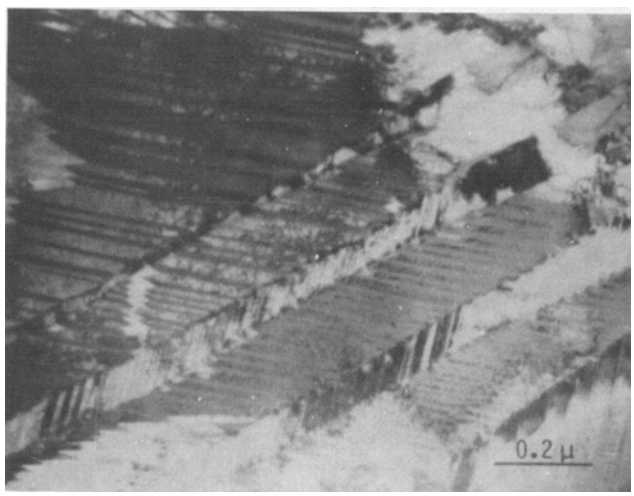

(*c*)

Fig. 7—Microstructure of material cooled at 250 Ks^{-1}. (*a*) Bright-field illumination showing prior γ grain boundaries and substructure within the prior γ grains. (*b*) Polarized light illumination showing the α'' martensitic structure within the prior γ grains. (*c*) Transmission electron micrograph showing the highly twinned nature of the α'' martensite.

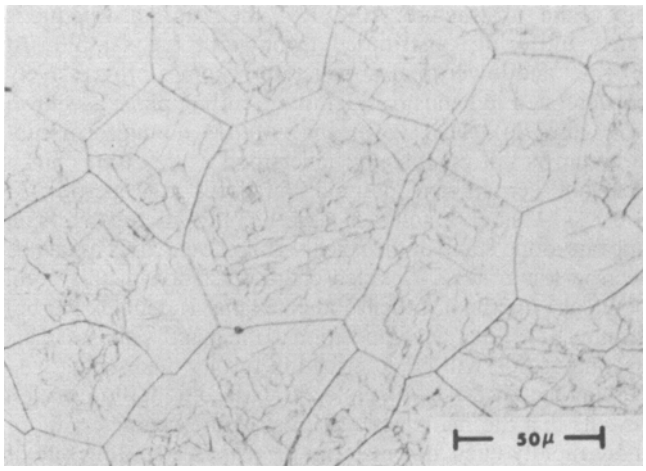

(a)

(b)

Fig. 8 — Microstructure of material cooled at 20 Ks^{-1}. (*a*) Bright-field illumination showing the formation of a subgrain network within the prior γ grains. (*b*) Scanning electron micrographs showing that the subgrain boundaries are made up of rows of individual dislocation etch pits.

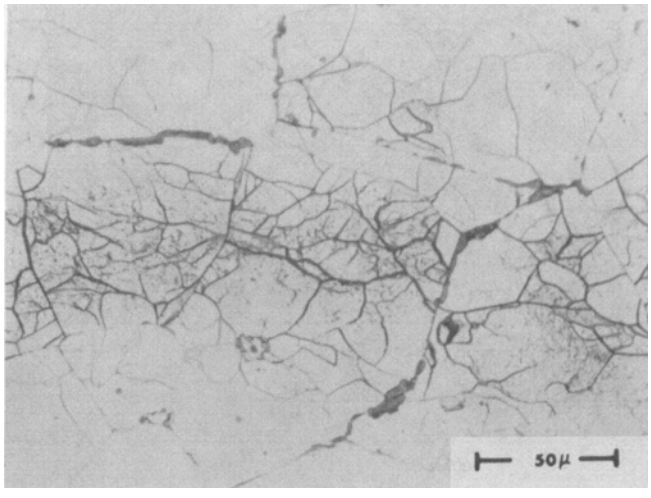

(a)

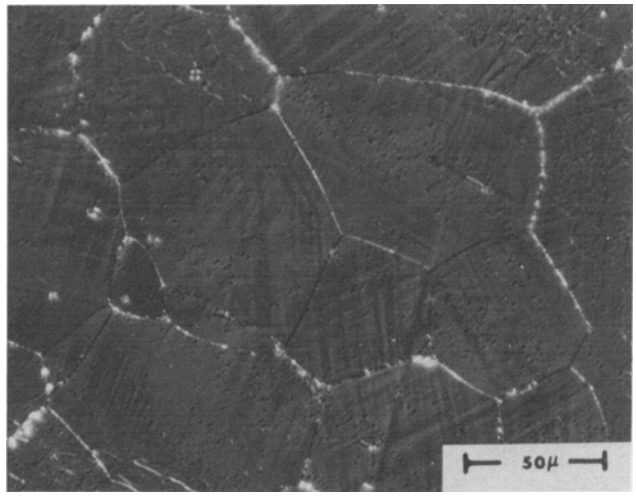

(b)

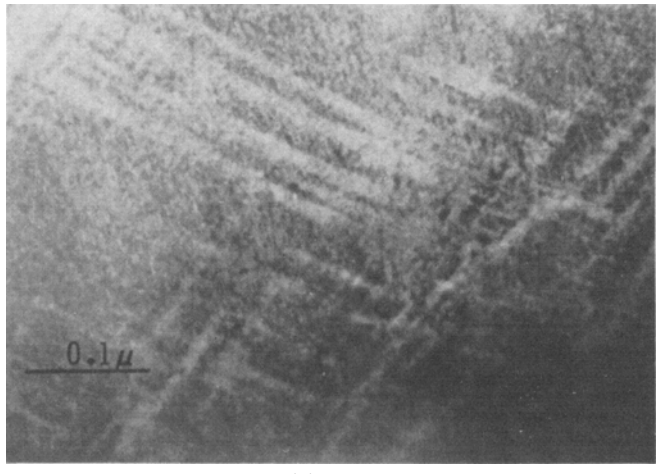

(c)

Fig. 9 — Microstructure of material cooled at 0.83 Ks^{-1}. (*a*) Bright-field illumination showing substructure banding and dark etching microconstituent at prior γ grain boundaries. (*b*) Polarized illumination showing α'' martensitic structure. (*c*) Transmission electron micrograph showing very fine modulated structure in the α'' phase.

shown in Figure 8(a). Higher magnification scanning electron microscopy reveals that the subgrain boundaries are made up of rows of dislocation etch pits as shown in Figure 8(b). Apparently the lower cooling rates permit time for the quenching induced strains to be relieved by nonconservative dislocation movement and the formation of low angle boundaries. The X-ray diffraction results also indicated that quenching induced strain decreases with decreasing cooling rate. No significant changes in the α martensite structure are revealed by either polarized light or transmission electron microscopy in the high cooling rate regime, corresponding to the observation that neither mechanical nor corrosion behavior changes over this range of cooling rates.

In the intermediate cooling rate regime, substantial microstructural changes occur. The primary change observed by optical metallography is a change in the morphology of the substructure. At 20 Ks^{-1} the subgrain structure is fairly uniformly distributed throughout the sample. At 10 Ks^{-1} and lower this substructure becomes progressively concentrated in bands parallel to the rolling plane as shown in Figure 9(a). The significance of this nonuniform substructure is not completely understood at this time, but it does not seem to have an important effect on properties. At 0.8 Ks^{-1} a small amount of dark etching microconstituent appears along some of the prior γ grain boundaries as can be seen in Figure 9(a). Detailed characterization of this grain boundary microconstituent indicates that it denotes the beginning of cellular decomposition to the α and γ phases. This decomposition will be described in further detail when discussing the lowest cooling rates. Polarized light illumination reveals that the martensitic microstructure characteristic of more rapidly quenched material persists to a cooling rate of 0.8 Ks^{-1}. The sharp resolution of the martensitic bands

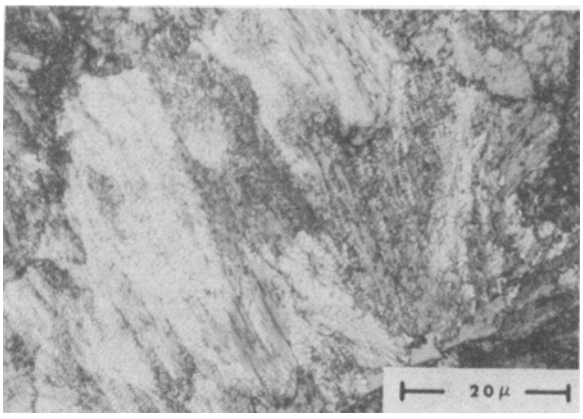

(a)

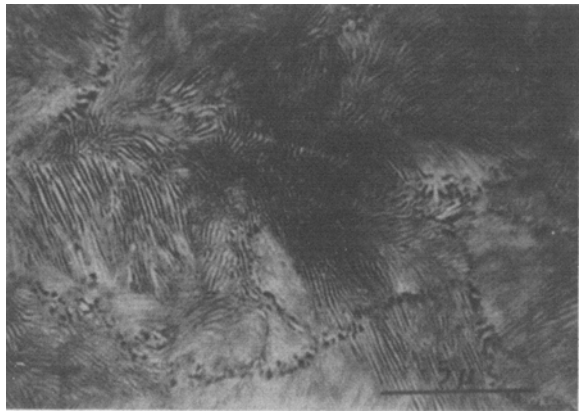

(b)

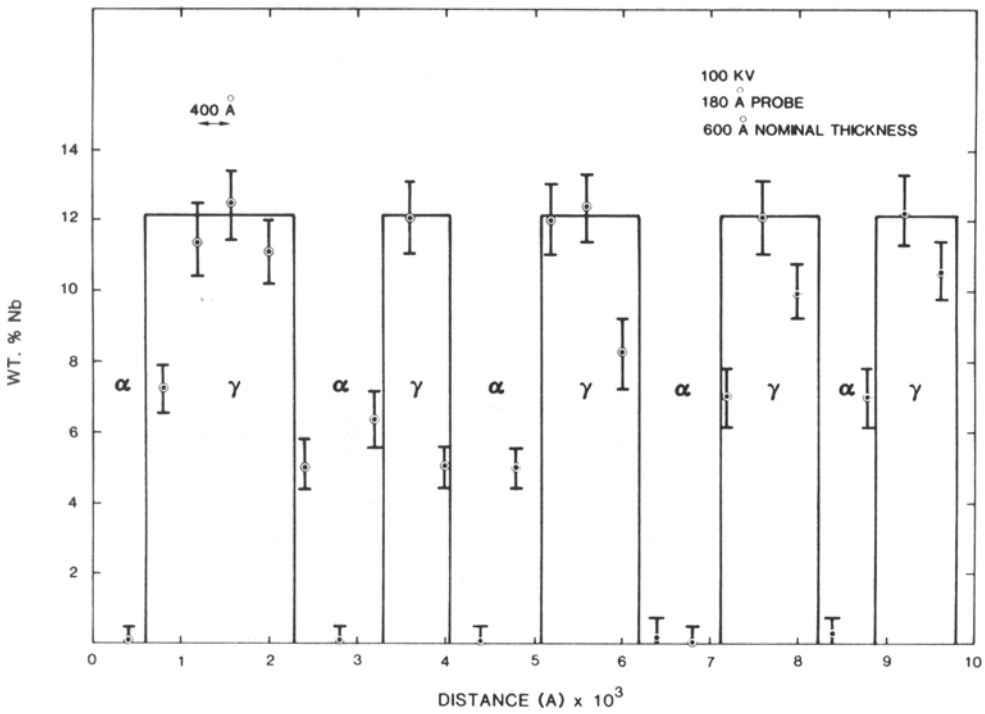

(c)

Fig. 10—Microstructure of material cooled at 0.04 Ks^{-1}. (*a*) Bright-field illumination showing fine lamellar structure. (*b*) Scanning electron micrographs showing details of the lamellar structure. (*c*) Plot of niobium content across several α and γ_{1-2} lamellae as determined by analytical electron microscopy.

seems to degrade somewhat with decreasing cooling rate as shown in Figure 9(b). The most dramatic microstructural change which occurs in this regime, however, is the occurrence of a very fine modulated structure within the α'' martensite as shown in Figure 9(c). This feature is not immediately obvious at higher cooling rates, such as that shown in Figure 7(c). The characteristic dimension of these modulations appears to be approximately 50 Å, making them visible only by transmission electron microscopy and potentially very potent strengtheners. These modulations become more obvious with decreasing cooling rate and are very prominent at 0.8 Ks^{-1}. It appears that this structure is responsible for the increase in hardness and strength that occurs with decreasing cooling rate in the intermediate cooling rate regime. These observations are also consistent with the broadening in X-ray diffraction peaks that is observed in this range of cooling rates and is interpreted as being due to either coherent precipitates or compositional modulations.

At low cooling rates a completely different two-phase lamellar microstructure is observed as shown in Figure 10(a). The two-phase nature of this microstructure is barely resolvable by optical metallography, the lamellar spacing being on the order of 0.5 μm. The lamellar morphology can be more clearly resolved using scanning electron microscopy as shown in Figure 10(b). Transmission electron microscopy and electron diffraction confirms that the two phases are α and γ. Quantitative elemental analyses of these phases in the analytical electron microscope indicates their compositions to be <0.5 wt pct Nb and 12.0 ∓ 1.2 wt pct Nb, respectively, as shown in Figure 10(c).[17] These results are consistent with the phase identifications and compositional inferences made from the X-ray diffraction data.

E. *Effects of Cooling Rate on Response to Subsequent Aging*

The effects of cooling rate on age hardening response are shown in Figure 11. Materials quenched at high rates age harden between 298 K and 673 K, and overage at temperatures in excess of 673 K as has been previously reported for rapidly quenched material.[7] Samples cooled at intermediate rates exhibit progressively higher initial hardnesses and lower initial age hardening response with decreasing cooling rate. During the later stages of age hardening and overaging, however, the hardnesses of these materials are essentially equivalent to those of very rapidly quenched material. Samples cooled at low rates have the highest initial hardnesses, but cannot be age hardened. They undergo a small amount of softening at aging temperatures in excess of 723 K.

X-ray diffraction measurements and metallographic observations indicate that the microstructural effects which lead to property changes during aging are similar, but probably not in all cases identical, to those which occur with decreasing quenching rate. Low temperature aging (473 to 573 K) of rapidly quenched material produces a sharpening of the X-ray diffraction peaks and an increase in the amount of substructure present within the prior γ grains as can be seen by comparing Figures 6(a) and 7(a) with Figures 12(a) and 12(b), respectively. The diffraction data indicate that quench induced strains are at least partially relieved during low temperature aging. The amount of substructure observed in the most rapidly quenched and aged samples,

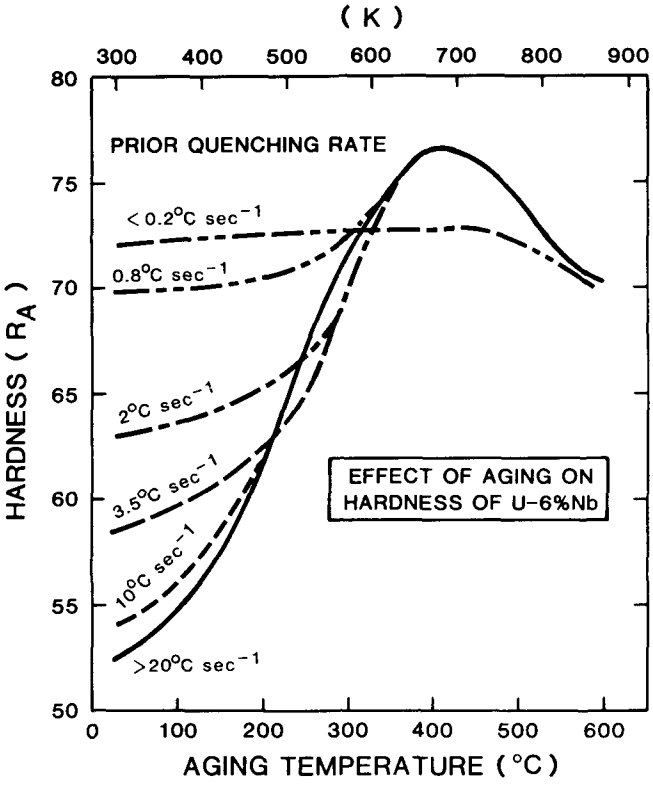

Fig. 11 — Effect of prior cooling rate and aging temperature on hardness.

however, is substantially lower than that observed in material cooled at 20 Ks^{-1} and not aged, as can be seen by comparing Figures 12(b) and 8(a). In addition, the substructure produced by aging is fairly uniform rather than banded as is characteristic of cooling at intermediate rates.

Hardening induced by aging results in much less broadening of diffraction peaks than does hardening induced by slow cooling, as can be seen by comparing Figures 12(a) and 6(d), the diffraction patterns from materials having equivalent hardness. This suggests that different mechanisms might be responsible for these strengthening effects, but a detailed transmission electron microscopy study would be required to elucidate these differences. Age hardening does not occur in samples cooled at very low rates because the α and γ_{1-2} phases produced at these cooling rates are not supersaturated with niobium.

Overaging of material cooled at intermediate and high rates occurs by cellular decomposition to the α and γ_{1-2} as has been previously reported for rapidly quenched material.[7,16] This cellular decomposition nucleates along the prior γ grain boundaries as shown in Figure 13 and progresses by the movement of essentially planar transformation interfaces. This reaction begins at approximately 623 K and is complete at approximately 723 K over this entire range of prior quenching rates. X-ray diffraction indicates that the initial product of this cellular decomposition consists of essentially pure α-uranium plus γ_{1-2} containing less than 15 wt pct Nb. With continued overaging, however, the γ phase diffraction peaks decrease in intensity, broaden, and shift to higher angles, while the α phase diffraction peaks increase slightly in intensity, as shown in Figures 14(a) and 14(b). The intermediate niobium content γ_{1-2} phase is transforming to niobium rich γ_2 phase plus additional α phase.

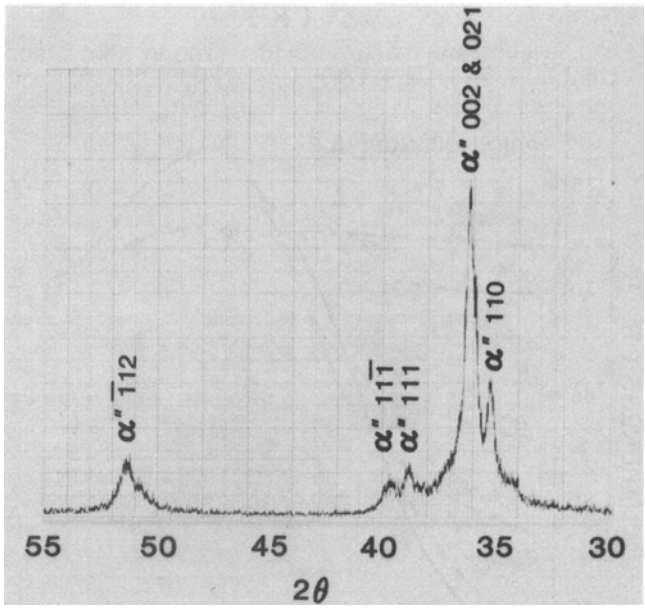

(*a*)

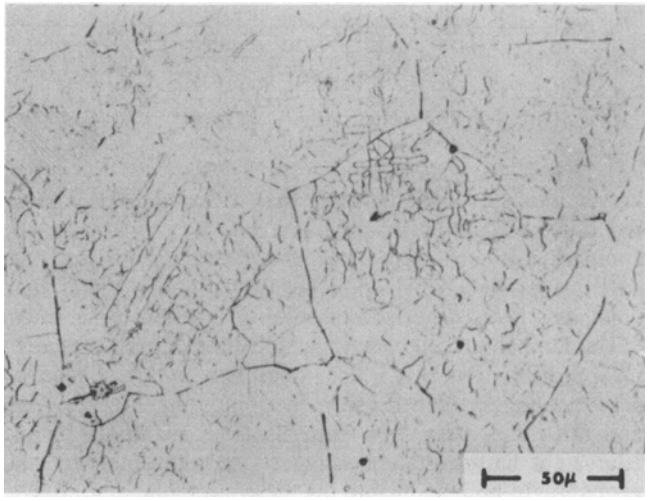

(*b*)

Fig. 12 — X-ray diffraction pattern and microstructure of material cooled at 250 Ks^{-1} and aged at 573 K for 6 h showing sharpening of diffraction peaks and development of substructure.

Aging at 723 and 873 K for six hours results in average apparent γ phase niobium contents of 18 and 26 wt pct, respectively, as determined by lattice parameter measurements. Presumably this would increase to the ~54 pct Nb composition of equilibrium γ_2 if the samples were held at temperature for longer times. This transformation is qualitatively consistent with previous work, but the previous study indicates that it should not begin to occur until six hours at 773 K or 30 hours at 873 K.[12]

In samples cooled at low rates the γ_{1-2} phase which formed during cooling undergoes a similar transformation to $\alpha + \gamma_2$ on aging in the 723 K to 873 K range. The transformation is somewhat more sluggish in these samples, however. The average apparent γ phase niobium contents are 14 and 17 wt pct after aging for six hours at 773 K and 873 K, respectively.

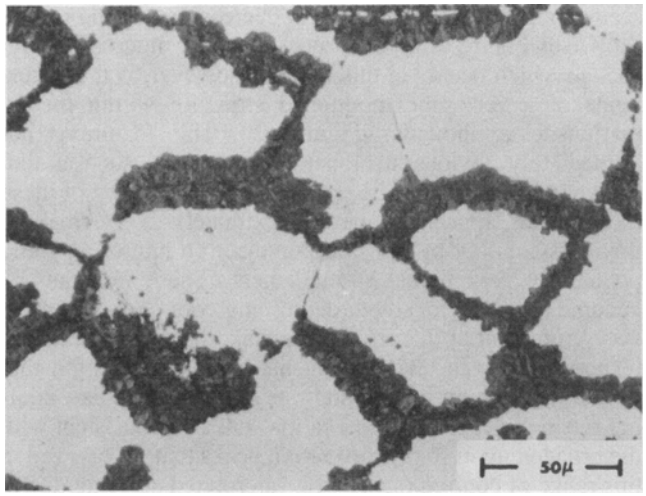

Fig. 13 — Microstructure of material cooled at 250 Ks^{-1} and aged at 673 K for 6 h showing cellular decomposition occurring along the prior γ grain boundaries.

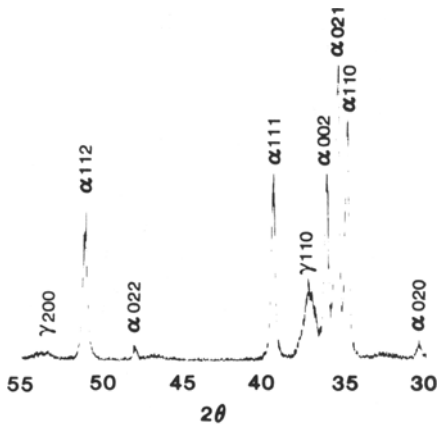

(*a*)

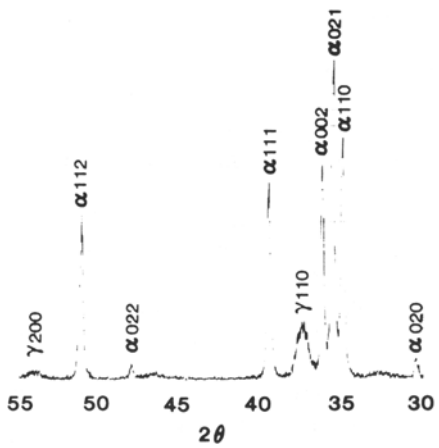

(*b*)

Fig. 14 — X-ray diffraction patterns of material cooled at 250 Ks^{-1} and aged at: (*a*) 773 K, (*b*) 873 K, for 6 h.

IV. DISCUSSION

A. *Cooling Rate–Microstructure–Property Relationships*

At high cooling rates diffusional transformations are completely suppressed and the γ_1 phase transforms martensitically to α'', a metastable variant of the α phase containing 6 pct niobium in supersaturated solid solution. This

extensively twinned thermoelastic martensite exhibits very low yield strength and high ductility. The low yield strength results from the fact that the twin boundaries in this material are highly mobile, as is typical of thermoelastic martensites.[18] Material in this condition exhibits much better corrosion resistance than unalloyed uranium due to the presence of 6 pct Nb in solid solution. In addition, the niobium supersaturation makes this material amenable to subsequent age hardening. The only influence of cooling rate in this regime is on the ability of dislocations to form subgrain networks and relieve quench induced strains (autorecovery). The formation of these subgrain boundaries, however, has essentially no effect on mechanical behavior, corrosion resistance, or age hardenability.

As cooling rate decreases from 10 Ks^{-1} to 0.8 Ks^{-1}, fine scale microstructural changes become increasingly apparent. The nature of these changes is not fully understood at this time, but present microstructural and X-ray diffraction observations are consistent with the hypothesis that spinodal decomposition is occurring in the γ_1 phase prior to its transformation to α''. The feasibility of spinodal decomposition in U-Nb alloys is indicated by the miscibility gap which occurs in the γ-phase above 920 K and extrapolates to 0 pct Nb at approximately 740 K (Figure 1). The spinodal boundaries cannot be calculated due to insufficient thermodynamic data, but it is entirely possible that the spinodal gap spans the 6 pct Nb composition at temperatures above the 363 K martensite start. Subsequent cooling of the compositionally modulated γ-phase would result in transformation either to modulated α'' (if magnitude of the niobium modulation is <2 pct) or to $\alpha'' + \gamma^\circ$ (if the magnitude of the niobium modulation is >2 pct). The very small dimensions

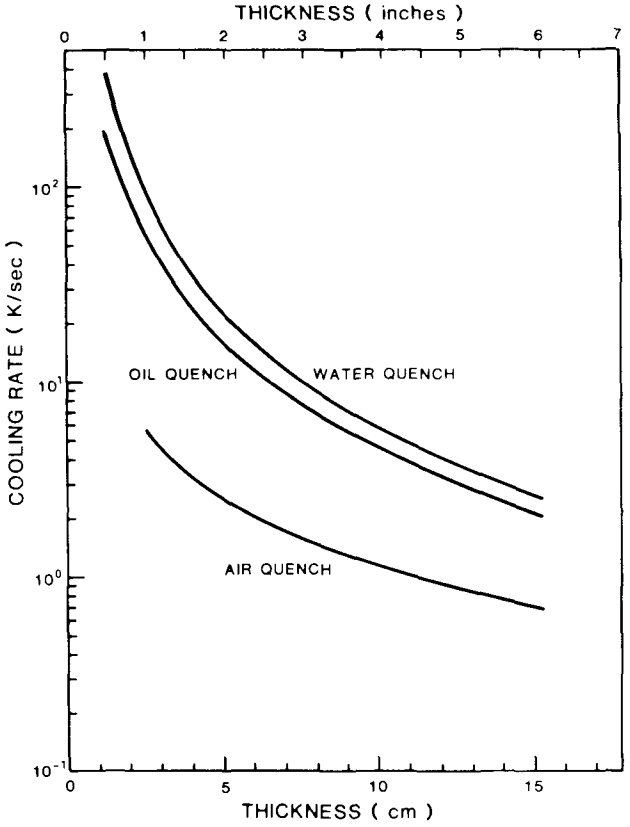

Fig. 15—Cooling rates at the centers of plates cooled in water, oil, and air.

(~50 Å) over which these compositional modulations occur make them very potent strengtheners. Hence, hardness and strength increase dramatically at the expense of ductility with decreasing cooling rate. These large changes in mechanical properties are accompanied by a slight decrease in corrosion resistance, probably because the relatively small differences in niobium content associated with the compositional modulations provide very fine scale anodic and cathodic regions in the material. Age hardenability is changed only in that the material appears to have been partially aged during the quenching process. Despite the fact that the X-ray diffraction results suggest that the mechanisms of hardening due to subcritical quenching and hardening due to aging are not identical, both hardening mechanisms are obviously due to diffusionally controlled, very fine microstructural changes driven by the thermodynamic instability of supersaturated phases. Hence, these processes would be expected to have a similar effect on the mechanical behavior.

At low cooling rates the γ_1 phase undergoes cellular decomposition to $\alpha + \gamma_{1-2}$. This two-phase microstructure is substantially coarser than the modulated microstructure produced at higher cooling rates, and becomes still coarser with decreasing cooling rate. Hence, in this regime, yield strength decreases and ductility increases with decreasing cooling rate.* Despite the substantial decrease in yield strength with decreasing cooling rate, hardness and ultimate strength decrease very slowly because the strain hardening exponent of material with the $\alpha + \gamma_{1-2}$ microstructure is approximately 30 pct higher than that of material with the $\alpha'' + \gamma^\circ$ microstructure (based on fitting the true stress–true strain curves of materials with comparable yield strengths to the equation $\sigma = \kappa\varepsilon^n$). The $\alpha + \gamma_{1-2}$ microstructure results in substantially less corrosion resistance than any of the other microstructures studied because the α phase contains essentially no niobium in solid solution and because the large difference in niobium concentration between the α and γ_{1-2} phases creates microscopic anodes and cathodes of substantially different electrochemical potential. Material in this condition cannot be age hardened because the α phase is not supersaturated with niobium.

*Due to slight differences in the cooling rates of nominally identically treated samples, the transition in mechanical properties is reported as occurring between 0.18 Ks^{-1} and 0.040 Ks^{-1} while the transitions in microstructure, corrosion resistance, and aging response are reported as occurring between 0.83 Ks^{-1} and 0.18 Ks^{-1}. Metallographic and X-ray diffraction samples taken from broken tensile bars which had been nominally cooled at 0.18 Ks^{-1} revealed $\alpha'' + \gamma^\circ$ microstructures rather than the expected $\alpha + \gamma$ microstructures, which indicate that these tensile bars had actually been cooled at a slightly greater rate. It is apparent from this that the transition in microstructure and resulting properties occurs abruptly at a cooling rate slightly above 0.18 Ks^{-1}. This effect is due to the slightly different sizes of the specimens and not the solution or aging treatments.

B. *Section Size–Quench Medium Effects*

A heat-transfer cooling rate model was written to determine what microstructures and properties would be obtained in actual industrial scale samples. The model solves Fourier's Second Law

$$\frac{\partial T}{\partial t} = \alpha \frac{\partial^2 T}{\partial X^2} \qquad [1]$$

where T is absolute temperature, t is time, X is distance, and α is the thermal diffusivity. ($\alpha = K/\rho Cp$ where K is the

thermal conductivity, ρ is the density, and Cp is the specific heat.) Equation [1] was solved for the case of quenching a semi-infinite plate of known thickness in various quenching media including air, oil, and water. Cooling was assumed to occur by heat conduction through the fluid only (forced convection was not permitted). The cooling rate (calculated from 973 K to 873 K) at the plate midpoint is plotted as a function of thickness for the various quenching media in Figure 15. The water quench obviously produces the highest cooling rates. The cooling rates in oil and air are factors of 1.5 and over 10 times slower, respectively, than those in water. The cooling rates calculated by the model are consistent with those measured in the experimental bars.

A precise comparison of calculated and measured cooling rates is not possible since the calculations are for plates (one dimensional heat flow) and the experimental measurements were from bars (two-dimensional heat flow). However, the experimental and calculated cooling rates are consistent with respect to the relative quenching power of the various quenching media.

It can be seen that cooling rates of 20 Ks^{-1} (sufficient to obtain fully martensitic microstructures) can be obtained in 50 mm thick plates by water quenching or 40 mm thick plates by oil quenching. If some amount of hardening during the quench and a small decrease in corrosion resistance can be tolerated, even thicker plates can be quenched, or thinner plates can be air cooled. Since corrosion resistance does not substantially decrease above a cooling rate of 2.0 Ks^{-1}, corrosion resistant plates can be obtained by techniques as simple as air cooling, where a surface cooling rate greater or equal to 2.0 Ks^{-1} is obtainable in virtually any plate thickness.

V. CONCLUSIONS

1. Cooling rates greater than 20 Ks^{-1} cause the γ_1 phase to transform to α'' martensite. This niobium supersaturated thermoelastic martensite exhibits low tensile (~870 MPa) strength, high ductility (~30 pct), good corrosion resistance, and substantial age hardenability.
2. Cooling rates between 10 Ks^{-1} and 0.2 Ks^{-1} produce a very fine modulated structure within the α'' martensite. This structure has increased strength and decreased corrosion resistance slightly, and has little effect on the hardnesses which can be obtained by subsequent aging.
3. Cooling rates below 0.2 Ks^{-1} permit the γ_1 phase to decompose cellularly to a coarse lamellar microstructure of $\alpha + \gamma_{1-2}$. This structure exhibits moderate yield strength and ductility, but high hardness and ultimate strength. The absence of niobium supersaturation in the α phase and the substantial compositional differences between the α and γ_{1-2} phases make this structure substantially less corrosion resistant and impossible to age harden.
4. Fully martensitic microstructures with optimum ductility and corrosion resistance can be obtained in plates as thick as 50 mm by water quenching. Material with good corrosion resistance can be obtained in plates of virtually any thickness by air cooling.

ACKNOWLEDGMENT

This work was performed at Sandia National Laboratories and supported by the United States Department of Energy under contract number DE-AC04-76DP00789.

REFERENCES

1. A. N. Holden: *Physical Metallurgy of Uranium*, Addison-Wesley Publishing Co., Reading, MA, 1958.
2. W. D. Wilkinson: *Uranium Metallurgy*, Interscience Publishers, New York, NY, 1962, vol. 2.
3. J. J. Burke, *et al.*, eds., *Physical Metallurgy of Uranium Alloys*, Brook Hill Publishing Co., 1976.
4. K. H. Eckelmeyer: *Microstructural Science*, 1979, vol. 7, pp. 133-45.
5. Proceedings of American Society of Metals Conference on Metallurgical Technology of Uranium and Uranium Alloys, Gatlinburg, TN, 1981, in pub.
6. J. T. Waber: *Proc. of 2nd U.S. International Conference on Peaceful Uses of Atomic Energy*, 1958, vol. 6, pp. 204-14.
7. R. J. Jackson and D. V. Miley: *ASM Trans. Q.*, 1968, vol. 61, pp. 336-34.
8. R. P. Elliott: *Constitution of Binary Alloys*, First Supplement, McGraw-Hill Book Co., 1965, pp. 274-76.
9. K. H. Eckelmeyer: Sandia National Laboratory, Albuquerque, NM, unpublished research, 1980.
10. M. Anagnostidis, M. Colombie, and H. Monti: *J. Nucl. Mat'ls.*, 1964, vol. 11, pp. 67-76.
11. K. Tangri and D. K. Chaudhuri: *J. Nucl. Mat'ls.*, 1964, vol. 15, pp. 278-87.
12. R. J. Jackson: Report No. RFP-1613, Rockwell International, Rocky Flats Plant, Golden, CO, January 1971.
13. K. H. Eckelmeyer and F. J. Zanner: *J. Nucl. Mat'ls.*, 1977, vol. 67, pp. 33-41.
14. J. Gurland and J. Plateau: *Trans. ASM*, 1963, vol. 56, pp. 442-54.
15. R. J. Jackson: Report No. RFP-1683, Rockwell International, Rocky Flats Plant, Golden, CO, December 1970.
16. C. D'Amato, F. S. Saraceno, and T. B. Wilson: *J. Nucl. Mat'ls.*, 1964, vol. 12, pp. 291-304.
17. A. D. Romig, Jr.: in *Proc. 16th Annual Microbeam Analysis Society*, R. H. Geiss, ed., San Francisco Press, San Francisco, CA, 1981, pp. 249-57.
18. R. A. Vandermeer, D. A. Carpenter, W. G. Northcutt, and J. C. Ogle: *Proceedings of an Int'l. Conf. on Solid → Solid Phase Transformations*, H. I. Aaronson, D. E. Laughlin, R. F. Sekerka, and C. M. Wayman, eds., TMS-AIME, Warrendale, PA, 1982, pp. 1299-1303.